Failed-transition outbursts in black hole low-mass X-ray binaries

K. Alabarta [1,2]★ D. Altamirano,[1] M. Méndez,[2] V. A. Cúneo [3,4] F. M. Vincentelli [1]
N. Castro-Segura,[1] F. García,[2] B. Luff[1] and A. Veledina [5,6,7]

[1]*School of Physics and Astronomy, University of Southampton, Southampton SO17 1BJ, UK*
[2]*Kapteyn Astronomical Institute, University of Groningen, PO Box 800, NL-9700 AV Groningen, the Netherlands*
[3]*Instituto de Astrofísica de Canarias (IAC), Vía Láctea s/n, E-38205 La Laguna, S/C de Tenerife, Spain*
[4]*Departamento de Astrofísica, Universidad de La Laguna, E-38205 La Laguna, S/C de Tenerife, Spain*
[5]*Department of Physics and Astronomy, University of Turku, FI-20014 Turku, Finland*
[6]*Nordita, KTH Royal Institute of Technology and Stockholm University, Roslagstullsbacken 23, SE-10691 Stockholm, Sweden*
[7]*Space Research Institute of the Russian Academy of Sciences, Profsoyuznaya Str 84/32, Moscow 117997, Russia*

ABSTRACT

Black hole low-mass X-ray binaries (BH LMXBs) evolve in a similar way during outburst. Based on the X-ray spectrum and variability, this evolution can be divided into three canonical states: low/hard, intermediate, and high/soft state. BH LMXBs evolve from the low/hard to the high/soft state through the intermediate state in some outbursts (here called 'full outbursts'). However, in other cases, BH LMXBs undergo outbursts in which the source never reaches the high/soft state, here called 'failed-transition outbursts' (FT outbursts). From a sample of 56 BH LMXBs undergoing 128 outbursts, we find that 36 per cent of these BH LMXBs experienced at least one FT outburst, and that FT outbursts represent ∼33 per cent of the outbursts of the sample, showing that these are common events. We compare all the available X-ray data of full and FT outbursts of BH LMXBs from *RXTE/*PCA, *Swift/*BAT, and MAXI, and find that FT and full outbursts cannot be distinguished from their X-ray light curves, hardness–intensity diagrams, or X-ray variability during the initial 10–60 d after the outburst onset. This suggests that both types of outbursts are driven by the same physical process. We also compare the optical and infrared (O/IR) data of FT and full outbursts of GX 339−4. We found that this system is generally brighter in O/IR bands before an FT outburst, suggesting that the O/IR flux points to the physical process that later leads to a full or an FT outburst. We discuss our results in the context of models that describe the onset and evolution of outbursts in accreting X-ray binaries.

Key words: accretion, accretion discs – black hole physics – X-rays: binaries.

1 INTRODUCTION

Low-mass X-ray binaries (LMXBs) are binary systems in which the primary component is a compact object, either a black hole or a neutron star, and the secondary component is a low-mass star, typically with a mass $<1\,M_\odot$. LMXBs with a black hole candidate as primary component are known as black hole LMXBs (BH LMXBs). The energy spectra of LMXBs can be described by two main components during outburst: a soft thermal component and a hard power-law component (e.g. Remillard & McClintock 2006; Belloni 2010). The soft thermal component is described by a multicolour disc blackbody model (Mitsuda et al. 1984) generally peaking at 0.1–1 keV depending on the spectral state (see Done, Gierliński & Kubota 2007, for a review). This is thought to be produced by a geometrically thin and optically thick accretion disc (Shakura & Sunyaev 1973). The hard power-law component is thought to be produced at the corona that, in some scenarios, is a region composed of hot electron plasma with temperatures from tens to hundreds of keV that surrounds the compact object and possibly the accretion disc (Sunyaev &

Truemper 1979; Sunyaev & Titarchuk 1980). The emission of this component is due to thermal Comptonization, by which the low-energy photons are inverse Compton scattered by the electrons in the corona (Sunyaev & Titarchuk 1980; Titarchuk 1994; Zdziarski et al. 2004; Done et al. 2007; Burke, Gilfanov & Sunyaev 2017).

During an outburst, BH LMXBs show different spectral and timing properties (e.g. van der Klis 1989, 2000; Méndez & van der Klis 1997; Homan & Belloni 2005; Remillard et al. 2006; Belloni 2010; Belloni, Motta & Muñoz-Darias 2011; Plant et al. 2014; Motta 2016). Taking into account these properties, different states have been defined. Although different classifications have been proposed, here we use the classification given by Homan & Belloni (2005), among others, which defines four spectral states. When the source is in the *low/hard state* (LHS), the X-ray spectrum is dominated by a thermal Comptonization component that can be described by a hard power-law with a high-energy cut-off (around 100 keV) related to the temperature of the electron plasma (see Done et al. 2007, for a review). A weak disc-blackbody component can also be detected in the energy spectrum (e.g. McConnell et al. 2002; Zdziarski et al. 2002; Capitanio et al. 2009; Alabarta et al. 2020). In the LHS, the power-density spectrum (PDS) is characterized by a strong broad-band noise component with a break frequency below
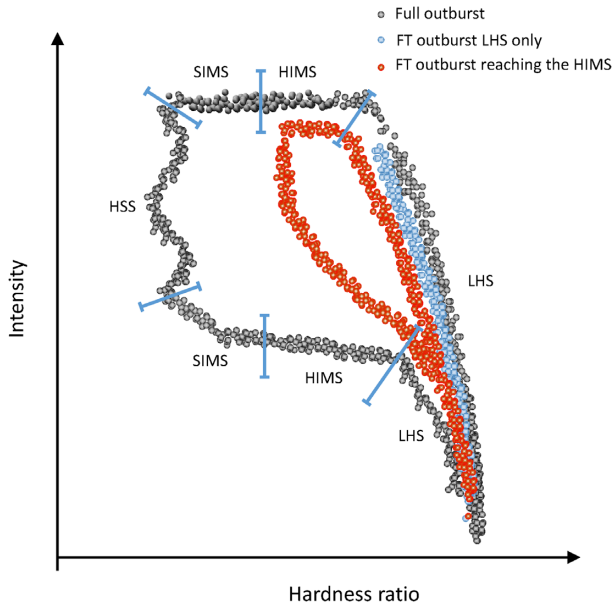
★ E-mail: k.alabarta@soton.ac.uk

Figure 1. Schematic HID of full (grey) and FT (red and blue) outbursts. The red track represents the sources that leave the LHS but do not reach the HSS and the blue track represents the sources that do not leave the LHS.

1 Hz and a high fractional rms amplitude (30–50 per cent; e.g. Belloni et al. 2005; Remillard & McClintock 2006; Muñoz-Darias, Motta & Belloni 2011; Motta 2016). Quasi-periodic oscillations (QPOs) can also be observed in this state with frequencies between 0.01 and 30 Hz (e.g. Casella et al. 2004; Belloni et al. 2005). The *high/soft state* (HSS) is characterized by an energy spectrum dominated by a soft thermal component due to an optically thick, geometrically thin accretion disc (Shakura & Sunyaev 1973). A very weak hard power-law component can also be detected (e.g. Capitanio et al. 2009; Alabarta et al. 2020). In the HSS, the fractional rms amplitude is less than 5 per cent and weak QPOs are sometimes detected (e.g. Casella et al. 2004; Rodriguez et al. 2004; Motta et al. 2011; Muñoz-Darias et al. 2011; Sriram, Rao & Choi 2013; Motta 2016). Between the LHS and the HSS, two intermediate states are defined considering the evolution of the X-ray variability: the *hard-intermediate state* and the *soft-intermediate state* (HIMS and SIMS, respecively; e.g. Homan & Belloni 2005; Belloni 2010). The HIMS is characterized by a broad-band noise fractional rms amplitude of 10–30 per cent (Muñoz-Darias et al. 2011; Motta et al. 2012) and sometimes QPOs can be detected (e.g. Casella et al. 2004; Belloni et al. 2005; Belloni & Stella 2014). The SIMS shows a fractional rms amplitude of a few per cent and type-A (in the 6.5–8 Hz frequency range) and type-B QPOs (in the 1–7 Hz frequency range) can also be found (e.g. Wijnands, Homan & van der Klis 1999; Homan et al. 2001; Casella et al. 2004; Belloni et al. 2005; Belloni & Stella 2014).

During a so-called canonical outburst, a system evolves through all the different spectral states in the following order: LHS → HIMS → SIMS → HSS → SIMS → HIMS → LHS. This evolution can be well traced using the hardness–intensity diagram (HID; e.g. Homan et al. 2001; Remillard et al. 2006), the hardness–rms diagram (Belloni et al. 2005), the rms–intensity diagram (Muñoz-Darias et al. 2011), and the power colour–colour (PCC) diagram (Heil, Uttley & Klein-Wolt 2015). The grey track in Fig. 1 shows a schematic representation of the track traced by a BH LMXB during an outburst in the HID. This pattern in the HID is known as the q-track. At the beginning, the source is in the LHS, in the right bottom part of the HID. In

this phase of the outburst, the source intensity increases without a big change of hardness, following a vertical line on the right of the HID. At some luminosity, the source starts the transition to the HSS moving to the left of the HID, following a horizontal branch without big changes of the source intensity. In this horizontal branch, the source enters the HIMS and the SIMS. When the source reaches the HSS state on the top left part of the HID, its intensity decreases at an approximately constant value of the hardness. From then on, the evolution reverses and the source returns to the intermediate states following a bottom horizontal branch of the HID. Finally, at the end of the outburst, the source goes through the LHS again. Several sources show this pattern in their outbursts, e.g. XTE 1550−564, GX 339−4, H1743−322, and GRO J1655−40 (Homan et al. 2001; Belloni et al. 2005; Fender, Homan & Belloni 2009; Dunn et al. 2010; Uttley & Klein-Wolt 2015). We call 'full outbursts' to the outbursts that follow the full spectral evolution.

Despite the q-track pattern observed in many BH LMXBs, some sources undergo outbursts that do not show the complete spectral evolution. These kinds of outburst are known in the literature as 'hard-only state outbursts' (Tetarenko et al. 2016), 'low/hard state outbursts' (Belloni et al. 2002), 'failed outbursts' (e.g. Capitanio et al. 2009; Curran & Chaty 2013), or 'failed state transition outbursts' (Bassi et al. 2019). According to the track traced on the HID, the 'failed outbursts' can be divided in two groups. The first group corresponds to sources that remain in the LHS during the whole outburst (e.g. Hynes et al. 2000; Brocksopp et al. 2001; Belloni et al. 2002; Brocksopp, Bandyopadhyay & Fender 2004; Curran & Chaty 2013), while the sources belonging to the second group make the transition to the intermediate states without reaching the HSS (e.g. in't Zand et al. 2002; Capitanio et al. 2009; Ferrigno et al. 2012). The tracks followed by these two types of 'failed outbursts' are represented with blue and red circles in Fig. 1, respectively. All 'failed outbursts', in addition, appear to reach fainter X-ray luminosity peaks than full outbursts (Tetarenko et al. 2016). Most of the names presented in the lines above to call this type of outbursts do not completely describe their real nature. 'Failed outbursts' may cause some confusion by giving the impression that the source did not undergo into outburst. The names of 'hard-only state outbursts' and 'low/hard state outbursts' give the impression that the source never leaves the LHS. However, we have mentioned that some 'failed outbursts' made the transition to the HIMS. For simplicity, we propose the nomenclature 'failed-transition' outbursts (hereafter FT outbursts), similar to that used by Bassi et al. (2019).

Some studies analysed the differences between full and FT outbursts in radio wavelengths. Corbel et al. (2013) found the correlation between the X-ray and radio emission. The same correlation was also found only with the hard state emission of the source. Fürst et al. (2015) used new data to confirm this correlation and they found that the correlation is slightly different for the FT (2008, 2009, and 2013) than for the full outbursts. de Haas et al. (2020) found a flatter radio–X-ray correlation using FT outbursts of GX 339−4 than with full outbursts of the same source. They interpreted this flatter correlation as an inefficient coupling between the X-rays and radio emission mechanisms. They also suggested that this correlation could be used to predict the nature of the outburst at its early stages. However, Williams et al. (2020) studied the same correlation in the 2018 FT outburst of H 1743−322 and found that full and FT outbursts of this source show a similar correlation.

In this paper, we present the observational differences between full and FT outbursts using X-ray and O/IR data during the first days of the outbursts. The aim is to understand why some outbursts behave as full outbursts and some others as FT outbursts and, in particular,

whether it is possible to predict the type of outburst during the first days. After an exhaustive search of the X-ray archive and literature, we constrained our analysis of X-ray data to three BH systems that have enough observations during the rising part of the outburst: GX 339−4, H 1743−322, and GRS 1739−278. In addition, we also studied O/IR data of GX 339−4. In Section 2, we describe the source selection and the data analysis. In Section 3.1, we show the fraction of FT outbursts of our sample. In Section 3.2, we show the relation between the X-ray peak intensity of the outbursts and the time spent in quiescence between outbursts. In Sections 3.3, 3.4, and 3.5, we compare the observational X-ray light curves, HIDs, and PCC diagrams between FT and full outbursts. In Section 3.6, we analyse the observational differences between both types of outbursts of GX 339−4 in O/IR wavelengths during outburst and quiescence. Finally, in Sections 4 and 5, we discuss our results and present our conclusions.

2 DATA AND DATA ANALYSIS

2.1 Source selection

For our study, we selected 46 transient BH LMXBs from the WATCHDOG catalogue (Tetarenko et al. 2016) that showed at least one full or one FT outburst. In the cases where the outburst was not classified in the literature, we checked the spectral and timing properties of the source to decide whether they were consistent with those of full or FT outbursts, and hence included them in our study. If the spectral and timing properties were not enough to determine the nature of the outburst, the source was excluded. In addition to the 46 BH LMXBs studied by Tetarenko et al. (2016), we considered one more source (MAXI J1828−249) not included in that paper and nine further BH systems that went in outburst from 2016 until now. The final sample used in our study includes 56 sources that meet the above requirements (see Appendix A, in the supplementary online material).

2.2 X-ray light curves and HIDs

We used all the available data from the *Rossi X-ray Timing Explorer* (*RXTE*) Proportional Counter Array (PCA; for instrument information, see Zhang et al. 1993; Jahoda et al. 2006) for the selected sources. To calculate the hardness ratio (HR) we used the 16-s time-resolution Standard 2 mode data. For each of the five PCA detectors (PCUs), we calculated the HR defined as the 16.0–20.0 keV count rate divided by the count rate in the 2.0–6.0 keV band. We also calculated the intensity defined as the count rate in the 2–20 keV energy band. To obtain the count rates in these exact energy ranges, we made a linear interpolation between PCU channels. We then performed deadtime corrections, subtracted the background contribution in each band using the standard bright source background model for the PCA (version 2.1e1) and removed instrumental drop-outs to obtain the HR and intensity for each time interval of 16 s. We also took into account that the *RXTE* gain epoch changed with each new high voltage setting of the PCUs (Jahoda et al. 2006). To correct for this effect and the differences in effective area between the PCUs, we normalized our data to the Crab (method introduced by Kuulkers et al. 1994). Following this method, for each PCU we obtained the HR and intensity of the Crab, which is supposed to be constant, and after that we averaged the 16 s Crab HR and intensity for each PCU. Then, we divided them by the average Crab values that are closer in time and in the same *RXTE* gain epoch. We obtained the HR and intensity average over all PCUs and with that the average of HR and intensity for each interval of 16 s. Finally, we averaged the

HR and intensity for each ObsID separately. We also compared the *RXTE*/ASM, the 15–50 keV *Swift*/BAT[1] and the 2–20 keV MAXI light curves.[2]

2.3 Power colour–colour diagrams

The PCC diagrams of GX 339−4 analysed here were first presented by Heil et al. (2015). These authors obtained the so-called power colours, defined as the ratio of the broadband variability in two different frequency bands. They defined two power colours in the 2–16 keV energy band: PC1 as the ratio of the variability in the 0.25–2.0 Hz and 0.0039–0.031 Hz frequency bands; and PC2 as the ratio in the frequency bands 0.031–0.25 Hz and 2.0–16.0 Hz.

2.4 Optical and infrared light curves and colour–colour diagrams of GX 339–4

The optical and infrared (O/IR) data used in this paper come from the ANDICAM camera (DePoy et al. 2003) on the Small and Moderate Aperture Research Telescope System (SMARTS; Subasavage et al. 2010) and correspond to GX 339−4 (Buxton et al. 2012), since this is the only source with enough O/IR data for the purposes of this paper. The SMARTS light curves used in this paper were studied and presented in Buxton et al. (2012) and include the 2002–2010 time period. The SMARTS team also provided the O/IR light curves of the 2011–2015 period. The O/IR light curves consist of V, I, J, and H magnitude. Gaps in the data occur when the source is behind the Sun. We used the colours: $V - H$, $V - I$, $V - J$, $I - J$, $I - H$, and $J - H$. From them, we created the colour–magnitude diagrams (CMDs) comparing the colours defined with the O/IR band magnitudes.

3 RESULTS

3.1 Rate of FT outbursts

Based on the 56 sources that satisfy our selection criteria, showing 128 outbursts in the 1971–2021[3] time period (see Section 2 and Appendix A), we found that:

(i) 36 per cent of the sources showed at least one FT outburst (20 out of 56, see Appendix A for the list of sources). Fig. 2 shows, for each source that exhibits FT outbursts, the number of outbursts of each type.

(ii) 12 of the sources showed only FT outbursts (see Table A1, in the supplementary material).

(iii) 14 per cent of the sources show both full and FT outbursts (8 out of 56).

(iv) 33 per cent of the outbursts were catalogued (see references in Table A1) as FT outbursts (42 out of 128). Table A1 (supplementary material) contains the type of outburst of every outburst of the sources in our sample.

3.2 Quiescence times before full and FT outbursts

Full outbursts are brighter in X-rays than FT outbursts (Tetarenko et al. 2016). Assuming that the X-ray peak intensity depends on the amount of matter accumulated in the accretion disc and that the

---

[1] https://swift.gsfc.nasa.gov/results/transients/
[2] http://maxi.riken.jp/top/index.html
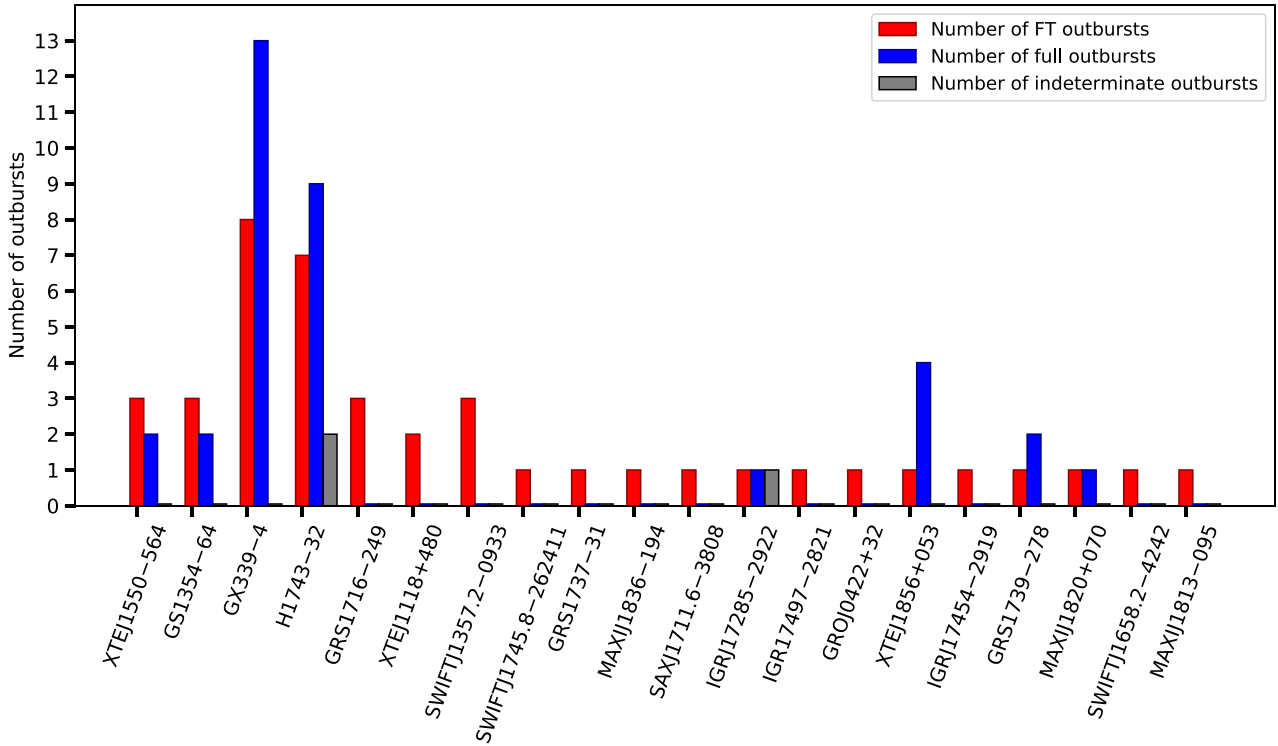[3] For completeness, we also considered an outburst of 1A 0620–00 that occurred in 1917.

Figure 2. Comparison between the number of FT and full outbursts in sources that exhibit both types of outbursts.

mass accretion rate from the companion star is constant, if a source spends more time in quiescence its accretion disc would accumulate more matter and, as a consequence, the following outburst would be brighter. Then, a source would spend more time in quiescence before a full outburst than before an FT outburst. Defining the quiescence time as the time difference between the onset of an outburst and the offset of the previous one in X-rays, we studied the relation between the quiescence time of full and FT outbursts and the *RXTE*/PCA peak intensity of the corresponding outburst. We used data from the sources GX 339−4, H 1743−322, and XTE J1550−564, since these were the only sources that underwent multiple outbursts of each type and the peak of the outbursts was observed with *RXTE*/PCA. To obtain the quiescence time, we used the begin and end times of the outbursts given by Tetarenko et al. (2016). Fig. 3 shows the relation between the quiescence time and the intensity peak of the outbursts of the sources mentioned before. We found that the three sources spent similar times in quiescence before FT and full outbursts. Only before two full outbursts (the 2002 of GX 339−4 and the 2007 outburst of H 1743−32) did the source spend a longer time in quiescence compared to the other outbursts.

3.3 X-ray light curves

As we mentioned before, full outbursts are brighter than FT outbursts (Tetarenko et al. 2016). What causes this difference in the maximum luminosity reached by each type of outburst can also make the light curves evolve in a different way from the beginning of the outburst for both types of outbursts. In order to study that, we compared, for all sources with enough available data, the rising part of the light curves of different FT and full outbursts of the same source. In order to do that, we considered the time of the beginning of the outbursts given in Tetarenko et al. (2016) and we then shifted all the
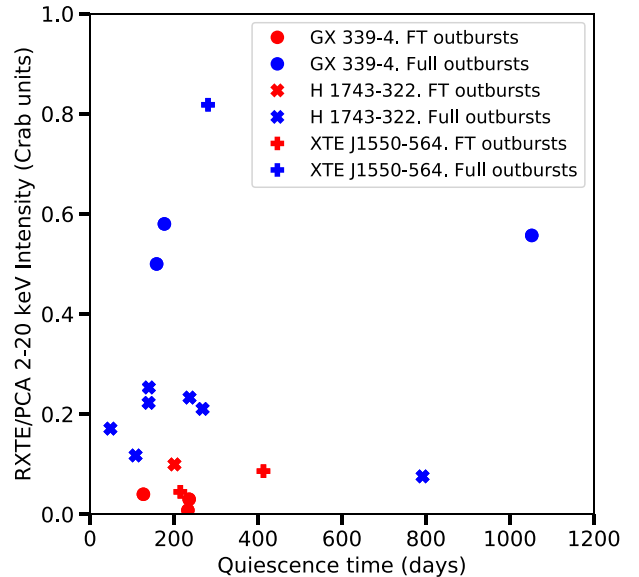

Figure 3. *RXTE*/PCA peak intensity versus quiescence time for the outbursts of GX 339−4, H 1743−322, and XTE J1550−564.

outbursts in time such that the start of all outbursts coincide in time. First, we compared the rising parts of both type of outbursts using data from pointed observations with *RXTE*/PCA. Then, we compared both type of outbursts using observations from *Swift*/BAT and MAXI, both all sky monitors. It is important to note that our results can be biased by the method used to determine the time of the beginning of the outbursts. Tetarenko et al. (2016) considered the beginning of an outburst as the first 3σ detection above the background using
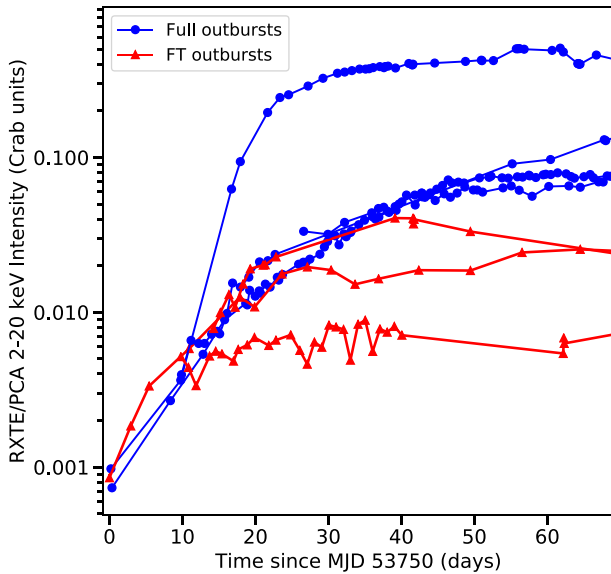
Figure 4. *RXTE*/PCA light curves of the beginning of the outbursts of GX 339−4.

different instruments. Because of that, the beginning of an outburst in a specific instrument can differ a few days from the value we used.

3.3.1 Comparing the rise of FT and full outbursts using X-ray light curves of RXTE/PCA

For the comparison of the rising parts of FT and full outbursts using *RXTE*/PCA observations, we focused on GX 339−4. This is the only source with multiple outbursts of each type with enough *RXTE*/PCA observations during the rising parts. Fig. 4 shows the comparison between *RXTE*/PCA light curves, where we plot four full outbursts in blue circles (2002, 2004, 2006, and 2009) and three FT outbursts in red triangles (2006, 2008, and 2009). We found that during the first ∼33 d, the light curves of FT and full outbursts evolved along similar tracks. After ∼33 d the flux of full outbursts continued increasing whereas the flux of FT outbursts started to decrease. The

only exception is the 2002 full outburst, whose intensity increased faster than the others.

3.3.2 Comparing the rise of FT and full outbursts using X-ray light curves of the all sky monitors Swift/BAT and MAXI

For the comparison of the rising parts of FT and full outbursts using all sky monitors, we used data from *Swift*/BAT and MAXI, given that most of the FT outbursts were too faint to be detected with *RXTE*/ASM. We focused on the sources GX 339−4, H 1743−322, and GRS 1739−278, since the three sources show full and FT outbursts bright enough to be detected with both instruments. As in the previous section, we considered the beginning of the outbursts defined by Tetarenko et al. (2016). However, in the case of H 1743−322, the source was first detected at higher energies than the energy band of MAXI and *Swift*/BAT, so the light curves are flat during the first days of the outburst. Therefore, we moved the beginning of the outbursts to the beginning of the rise of the outbursts.

Panel (a) of Fig. 5 shows the *Swift*/BAT light curves of GX 339−4, where three full outbursts in blue (2006, 2009, and 2014) and five FT outbursts in red (2006, 2008, 2009, 2013, and 2017) are plotted. The result was the same as with *RXTE*/PCA. During the first ∼30 d, the light curves of both types of outbursts followed similar tracks. After that, full outbursts were brighter than FT outbursts. The only exception was the 2013 FT outburst, which started to decay before the 33 d from the beginning. Panel (b) of Fig. 5 shows the 2–20 keV MAXI light curves of two full outbursts (2009 and 2014) and two FT outbursts (2013 and 2017) of GX 339−4. We see that both types of outburst overlap during the first ∼50 d.

Panel (a) of Fig. 6 shows the *Swift*/BAT light curves of six FT outbursts (2008, 2012, 2014, 2015, 2017, and 2018) and five full outbursts (2009, 2010, a second outburst in 2010, hereafter 2010b, 2013, and 2016) of H 1743−322. As we found for GX 339−4, it is not possible to distinguish between FT and full outbursts at the beginning of the outburst. Panel (b) of Fig. 6, on the other hand, shows the corresponding MAXI light curves of H 1743−322, including five FT outbursts (2012, 2014, 2015, 2017, and 2018) and four full outbursts (2010, 2010b, 2013, and 2016). The rising part of FT and full outbursts overlap during the first ∼20 d, which is the length of
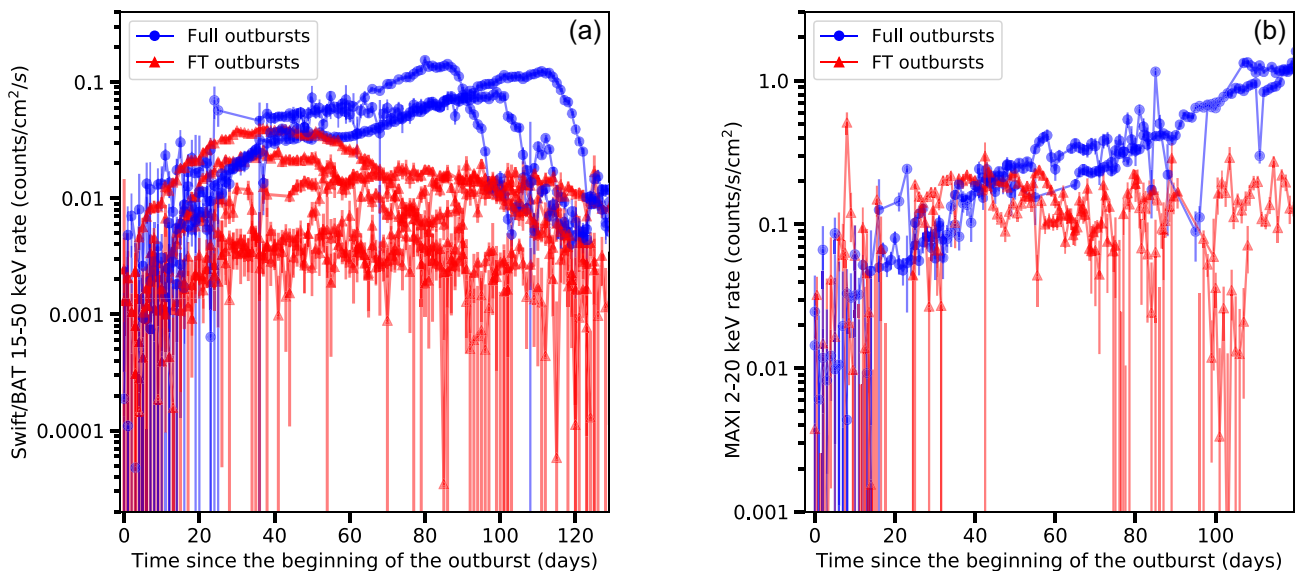
Figure 5. 15–50 keV *Swift*/BAT (panel a) and 2–20 keV MAXI (panel b) light curves of the beginnnig of the outbursts of GX 339−4.
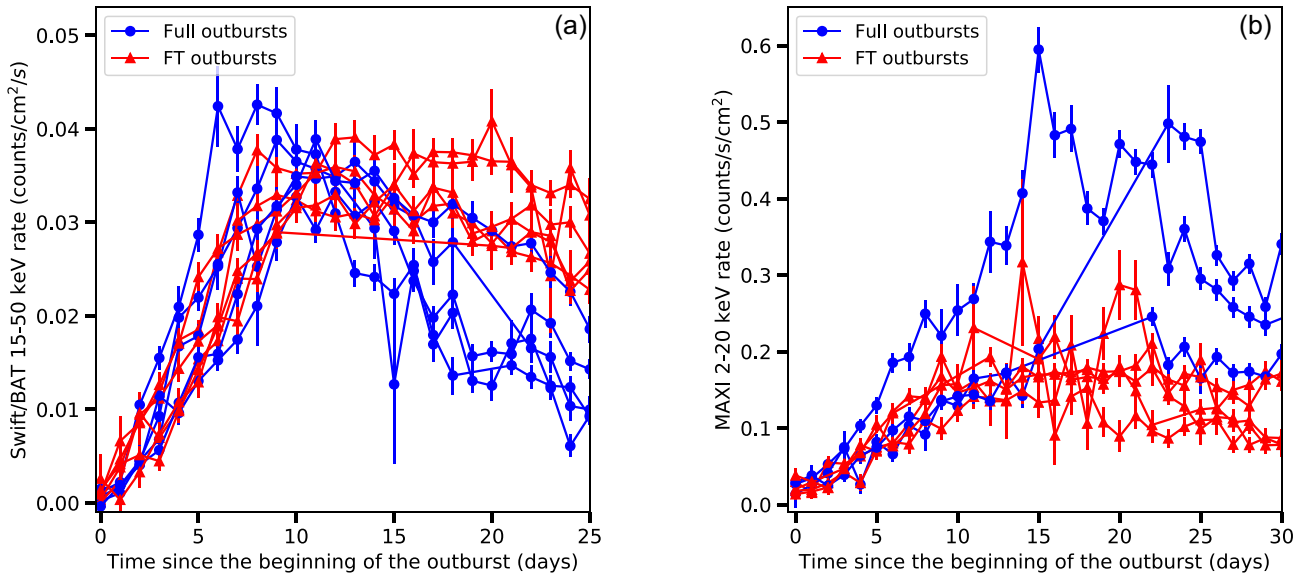
Figure 6. 15–50 keV *Swift*/BAT (panel a) and 2–20 keV MAXI (panel b) light curves of the beginning of the outbursts of H 1743−322.

the rising part of FT outbursts. The only exception is the 2010 full outburst of H 1743−322, whose intensity increased faster than the intensity of the other outbursts.

Panels (a) and (b) of Fig. 7 show, respectively, the *Swift*/BAT and MAXI light curves of the 2014 (full) and 2016 (FT) outbursts of GRS 1739−278. In contrast to GX 339−4 and H 1743−322, we found that the rising parts of the FT and full outbursts of GRS 1739−278 do not overlap during the first 30 d. The 2016 outburst is always fainter than the 2014 full outburst. This is due to the fact that the full outburst started to be observed when its intensity was at higher values than those reached by the FT outburst.

3.4 Comparing FT outbursts and full outbursts using the HID

As we mentioned in Section 1, FT outbursts do not show the full spectral evolution typical of BH LMXBs. This can be observed in the HID since FT outbursts do not follow the full q-track. Given that we observe the same behaviour for full and FT outbursts during the first ∼33 d in GX 339–4 light curves, we explored whether the track followed along the HID is also similar for both types of outburst. We compared the rise of full and FT outbursts using the *RXTE*/PCA HID of GX 339−4. As we mentioned in the previous section, GX 339−4 is the only source with enough observations during the rise of the outbursts to compare the track followed in the HID. Fig. 8 shows the rise of both types of outburst in the HID. Two full outbursts in blue (2004 and 2006) and three FT outbursts in red (2006b, 2008, and 2009) are plotted. We did not find significant differences between the rise of full and FT outbursts within error bars. All outbursts followed the same track along the HID.

For completeness, we also compared the rise and the decay of FT and full outbursts in the HID using *RXTE*/PCA data. The only FT outbursts with enough observations during the rise and the decay are the 2006, 2008, and 2009 outbursts of GX 339−4 and the 2003 outburst of XTE J1550−564. Panel (a) of Fig. 9 shows the HID of the FT outbursts of GX 339−4. We found that the three FT outbursts followed the same track along the HID. In addition, the rise and the decay overlapped in the HID. Panel (b) of Fig. 9 shows the HID of the 2003 FT outburst of XTE J1550−564. The rise and the decay of this outburst followed similar tracks in the HID, as it happens in GX 339−4.

As for full outbursts, we compared the rise and the decay of the 2005 outburst of GRO 1655−40 and the 2004 outburst of GX 339−4 since these are the only full outbursts with enough *RXTE*/PCA observations (Fig. 10). We found that the rise and the decay did not follow the same track along the HID, implying that the source is softer in the decay than in the rise of the outbursts, contrary to what we found for FT outbursts. Moreover, both the rise and decay phases of FT outbursts are located in the place of the rising phase of full outbursts.

3.5 Comparing the power spectra of full and FT outbursts using power colours

We explored whether the variability properties at the beginning of the outburst can affect the nature of the outburst. Fig. 11 shows the PCC diagram of the rise of full and FT outbursts of GX 339−4, obtained with *RXTE*/PCA observations. We found that FT outbursts did not show the whole track along the PCC diagram, but occupy a narrow area in the plot, which is the area corresponding to the LHS (Heil et al. 2015). This result was expected, since FT outbursts of GX 339−4 did not leave the LHS. If we only compare the rise of the outbursts, we found that the power colours of both type of outbursts overlap in the PCC diagram.

3.6 O/IR data of GX 339−4

We explored whether we can distinguish FT outbursts and full outbursts using O/IR data. In order to do that we used data from SMARTS. We focused on GX 339−4 since this is the most monitored BH LMXB in O/IR wavelengths. We divided our analysis in two parts. We first compared the rising parts of FT and full outbursts and, after that, we compared the periods of quiescence before FT and full outbursts.

3.6.1 O/IR data during outburst: light curves, O/IR correlations, and CMDs of FT and full outbursts

Fig. 12 shows the *RXTE*/PCA and *Swift*/BAT light curves (panel a) and O/IR light curves (panels b–e) of GX 339−4 of the time period 2002–2015. Five full (2002, 2004, 2006, 2009, and 2014) and four FT
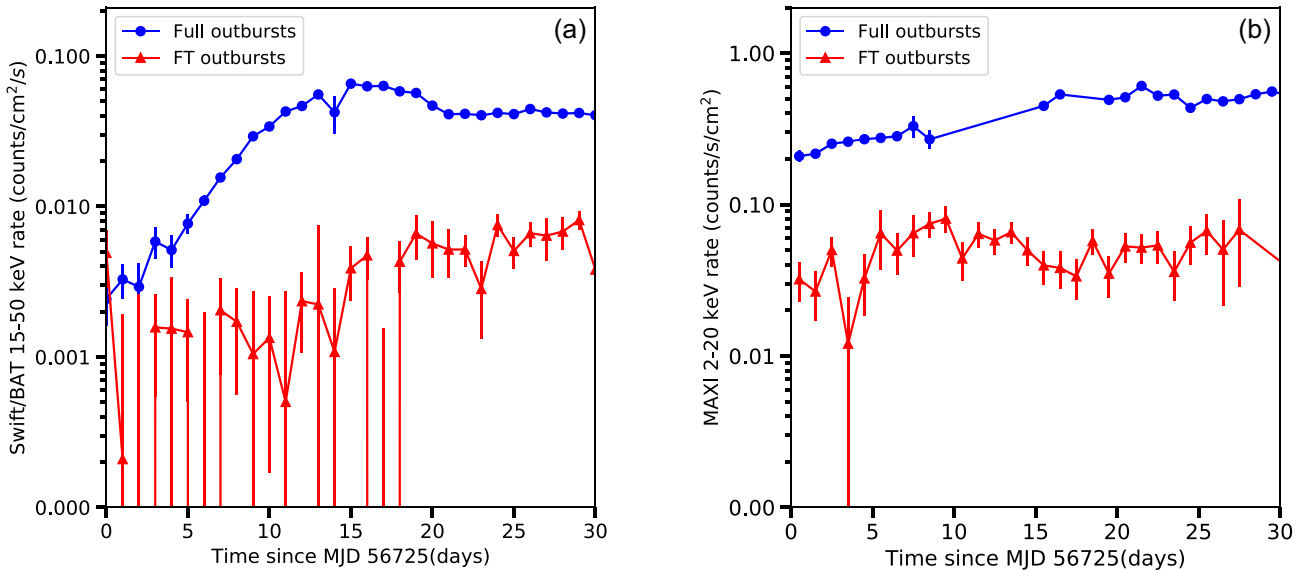
Figure 7. 15–50 keV *Swift*/BAT (panel a) and 2–20 keV MAXI (panel b) light curves of the beginning of the outbursts of GRS 1739−278.
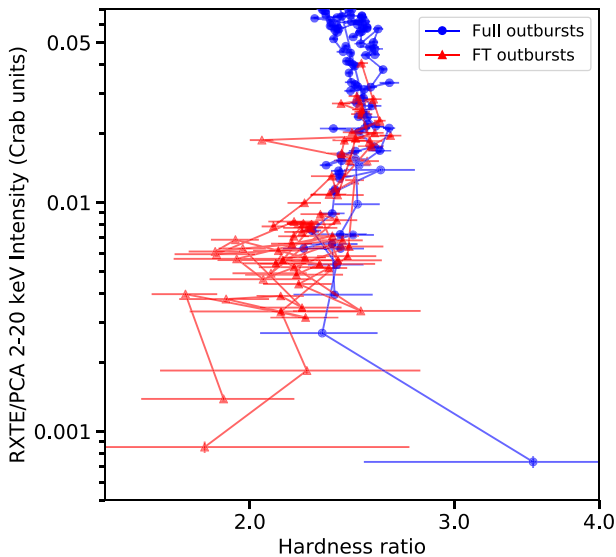

Figure 8. *RXTE*/PCA HID of 2004 (full), 2006 (FT), a second outburst in 2006 (full, 2006b), 2008 (FT), and 2009 (FT) outbursts of GX 339−4. The figure shows the rising and the end of the decaying parts of the outbursts.

outbursts (2006, 2008, 2009, and 2013; marked with green arrows) were observed during this period.

We found that the O/IR magnitudes of the peak of the 2008 and 2009 FT outbursts were lower than the magnitudes of the peaks of the full outbursts. This result is similar to that reported in Buxton et al. (2012) about the 2006 FT outburst. Moreover, the 2008 outburst is fainter than the 2006 and 2009 outbursts in X-rays, the same behaviour observed in O/IR wavelengths. We also found that the 2013 FT outburst peaked at similar magnitude as the full outbursts of GX 339−4.

We also compared the rising part of FT and full outbursts in O/IR wavelengths as we did in X-rays. Fig. 13 shows the rise of FT and full outbursts in the O/IR light curves, as we did in Section 3.3.1 with the *RXTE*/PCA light curves. We found that, at the beginning of the

O/IR outbursts, it is not possible to distinguish between full and FT outbursts.

In addition, we investigated the relation between the O/IR bands. Panel (a) of Fig. 14 shows the *V*-band against *H*-band magnitudes corresponding to the outbursts of the 2004–2014 time period. In agreement with Buxton et al. (2012), we observed two different branches in the plot. The top branch is described by a broken power law ($H \propto V^\alpha$) with the break located at $V \sim 16$ mag. The slope of the power law is larger than 1 from the faintest magnitudes to the break, and after the break the slope is less than 1. The bottom branch is well described by a single power law with a slope less than 1. Buxton et al. (2012) associated the top and the bottom branches with the LHS and the HSS, respectively. At the beginning of an outburst, GX 339−4 starts at the bottom left part of the diagram. During the LHS, the source follows the top branch until the top right part of the diagram. In the hard-to-soft state transition, the source leaves the top branch part and moves to the bottom branch, when the source reaches the HSS. In the bottom branch, the source evolves backwards to the bottom left side of the diagram. During the soft-to-hard transition, the source moves again to the top branch until the end of the outburst. Full outbursts of GX 339−4 follow this track. The FT outbursts of 2006, 2008, and 2009 fall on the top branch, as GX 339−4 was only seen in the LHS. We also found that the outburst of 2013, which is classified as an FT outburst, evolve from the top branch to the bottom branch.

Plots corresponding to the correlation between the *V* band and the *J* and *I* bands of the outbursts of GX 339−4 are on panels (c) and (e) in Fig. 14. In both cases, we see the two branches. When plotting the *V*-band versus the *I*-band magnitudes, we found that both branches are very close to each other and in the *V* band versus the *J* band the branches are more separated. In conclusion, we see that the two branches in Fig. 14 become more separated as we compare the *V* band to a band with longer wavelengths. Regarding the behaviour of full and FT outbursts, we also see that both types of outbursts fall in the top branch in the three cases.

Following the procedure performed with the HIDs with X-ray data, we compared the track followed by the rise of the full and FT outbursts of GX 339−4 in the CMD. Fig. 15 shows some representative CMD of the source. We found the same result as with the X-ray HIDs: the rising part of the full and FT outbursts lie
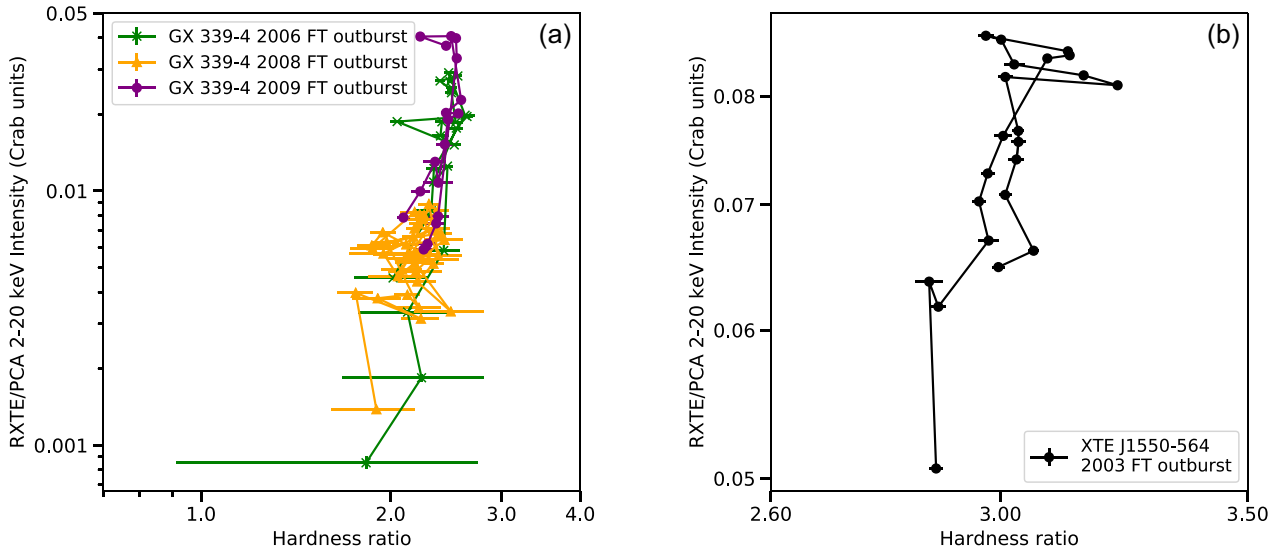
Figure 9. *RXTE*/PCA HIDs of the 2006, 2008, and 2009 FT outbursts of GX 339−4 (panel a) and the 2003 FT outburst of XTE J1550−564 (panel b). Both panels show the rising and decaying parts of the outbursts.
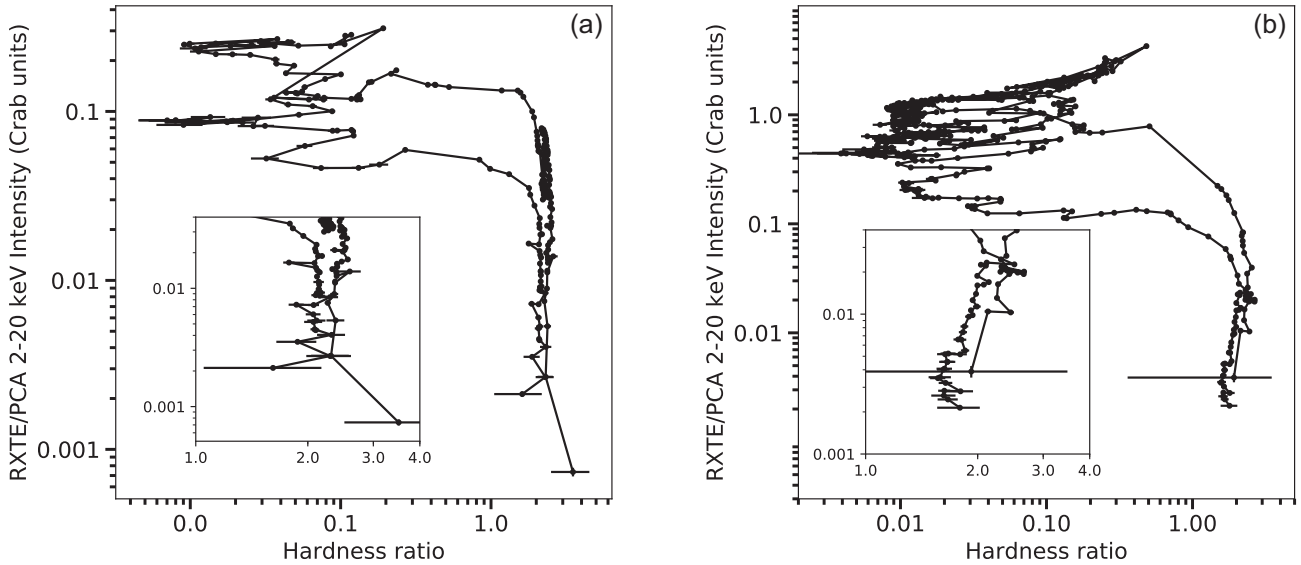

Figure 10. *RXTE*/PCA HIDs of the 2004 outburst of GX 339−4 (panel a) and the 2005 outburst of GRO 1655−40 (panel b), both full outbursts. The bottom right part of the diagram is zoomed.

on the same region of the CMDs for all the colours. This result is similar to that shown in Kosenkov et al. (2020), in which is reported that both types of outbursts follow the same track along the CMD. In addition to the data shown in Kosenkov et al. (2020), we show the CMDs of the 2013 (FT) and 2014 (full) outbursts of GX 339−4.

3.6.2 O/IR data during quiescence: light curves, O/IR correlations, and CMDs

GX 339−4 was also monitored in O/IR while the system was in quiescence in X-rays. In this paper, we define quiescence as the moments where no X-ray emission is detected from the source. This allowed us to study the O/IR light curves of GX 339−4 in these periods. When GX 339−4 reached the quiescence in X-rays after an outburst, the O/IR magnitudes were still decaying and, at some point,

they varied within an interval of ∼1 magnitude before starting to rise again. We also found that GX 339−4 did not have the same O/IR magnitudes while the source was in quiescence in X-rays before FT and full outbursts. In order to quantify this difference in brightness, we obtained the weighted average of the magnitude of the intervals where the O/IR magnitude varies within an interval of ∼1 mag that we previously mentioned. Between the end of the 2009 full outburst and the beginning of the 2013 FT outburst, the O/IR light curves show an optical outburst that was not detected in X-rays (Lewis, Russell & Shahbaz 2012; Maccarone, Russell & Glamorgan 2012). Just before the 2013 outburst, on MJD 56364, the *V* magnitude increased almost ∼2 mag in ∼2 d. Because of this behaviour, we decided to calculate the average of the O/IR magnitudes prior to the 2013 FT outburst after MJD 56364. These intervals are plotted with blue circles and red triangles in Fig. 12 and Appendix B (Supplementary online material).
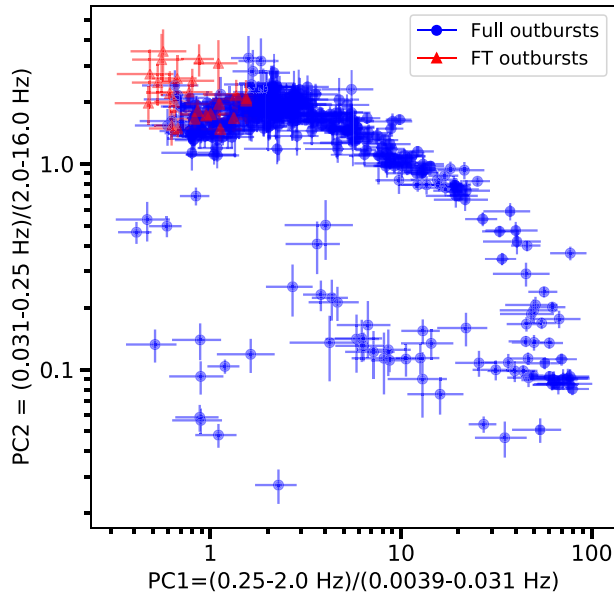
Figure 11. Power colours of full (1998, 2002, 2004, 2006b, and 2009b) and FT (2006, 2008, and 2009) outbursts of GX 339−4.

The average values obtained for these intervals are given in Table 1. We found that GX 339−4 was generally brighter in O/IR before undergoing an FT outburst than before a full outburst. In particular, before the 2008 outburst, GX 339−4 was always more than 1 mag brighter than before all the full outbursts. This can also be explained if the source did not go to quiescence before this outburst. Before the 2006 FT outburst, the source was ∼0.5 mag brighter than full outbursts in the V and I bands, but this difference was smaller than before the 2006b and 2009b full outbursts. The only exception occurred before the full outburst of 2014 when the source showed a brightness similar to that reached before FT outbursts in the O/IR bands.

We show the relation between the V and H bands during quiescence before FT and full outbursts in panel (b) of Fig. 14. We found that the periods of quiescence before full and FT outbursts that occurred before 2011 fall on the upper branch. The periods of quiescence prior to the outbursts of 2013 and 2014, on the other hand, fall on the lower branch. The same happens in the V-band versus I-band and V-band versus J-band plots (panels d and f of Fig. 14, respectively).

Fig. 16 shows the CMDs of the O/IR intervals corresponding to quiescence periods prior to FT outbursts (red triangles) and full outbursts (blue circles). We found that both intervals show the same values in terms of colours. The significant difference between them is their V magnitude (see also Section 4.4.2), as can be appreciated in Fig. 12.

We also estimated the temperature of the accretion disc during quiescence. Kosenkov et al. (2020) plots the line corresponding to a blackbody emission in Figs 4–11 (solid orange line). The intervals of quiescence before full outbursts (with $V \sim 19.25$–20 mag) correspond to a blackbody temperature of 8–10 kK. The temperatures of the quiescence intervals before the 2006, 2009, and 2013 outbursts range from ∼10 to ∼12.5 kK. The quiescence before the 2008 FT outburst is more brighter and its disc temperature is ∼15 kK, approximately.

4 DISCUSSION

We present the first systematic search for, and study of, the X-ray and O/IR data of FT and full outbursts. For all sources in our sample, we collected all the available data from *RXTE*/PCA,

MAXI and *Swift*/BAT to study the outbursts in X-rays. We found that 33 per cent of the outbursts of our sample are FT outbursts. We found that only three sources had enough data during the rise to compare both FT and full outbursts: GX 339−4, H 1743−322, and GRS 1739−278. When we compared the X-ray light curves of both types of outbursts, we found that during the first days of the outbursts of GX 339−4 and H 1743−322, the X-ray light curves of FT and full outbursts follow similar tracks. In contrast, the X-ray *Swift*/BAT and MAXI light curves of the 2014 (full) and the 2016 (FT) outbursts of GRS 1739−278 show that the 2014 outburst was always brighter than the 2016 FT outburst. Regarding the evolution along the HID and the PCC diagram, both types of outbursts of GX 339−4 follow the same track. For GX 339−4, the source in our sample showing a large number of full and FT outbursts, we were also able to combine the X-ray data with O/IR observations with the SMARTS telescope (the O/IR data for other sources is too sparse to be able to do detailed analysis). FT and full outbursts of GX 339−4 in the O/IR light curves and CMDs are similar. The only significant difference is that GX 339−4 was brighter in O/IR before FT outbursts than before full outbursts, while the source was in quiescence in X-rays.

4.1 Fraction of FT outbursts

We found that the 36 per cent of the black hole X-ray binaries included in this study showed FT outbursts, and that 33 per cent of the outbursts included in our sample were identified as FT outbursts. The percentage of FT outbursts that we found is similar to that obtained by Tetarenko et al. (2016). The reason for the small difference between the two results is that we did not include some of the sources of Tetarenko et al. (2016) and we updated the list of BH systems showing full or FT outbursts until 2021. The fact that three or four out of ten outbursts is an FT one tells us that FT outbursts are common events in BH LMXBs, as Tetarenko et al. (2016) pointed out.

4.2 FT and full outbursts in X-rays

Comparing the rising part of the outbursts of GX 339−4 and H 1743−322, we found that the X-ray light curves of FT and full outbursts overlap during the first 20–50 d, depending on the source and the instrument. After that, full outbursts continue brightening while FT outbursts faint. We also found that both types of outburst of GX 339−4 follow the same track along the HID during the rise of the outbursts, making impossible to predict their evolution during the first days. In addition, the behaviour of both type of outbursts in the PCC diagram is also similar. These three results suggest that the physical processes involved at the beginning of both types of outbursts are the same. It has been proposed that an LMXB makes a state transition if the source reaches a certain mass accretion rate (e.g. Esin, McClintock & Narayan 1997). Based on this hypothesis, the only difference between FT and full outbursts is that FT outbursts do not reach the mass accretion rate level needed to trigger the hard-to-soft state transition. Tetarenko et al. (2016) found that the luminosity at which the transition to the soft state occurs in the 2004 full outburst of GX 339−4 is ∼0.11 L_{edd}, and that the luminosity of FT outbursts is always equal or lower than this value. The question is why FT outbursts reach lower peak X-ray luminosities than full outbursts. If we assume that the accretion rate from the secondary star is constant, one possible explanation is that a longer quiescence time between outbursts could lead to a brighter outburst due to a larger accumulation of matter in the accretion disc. However, we found that there is no correlation between the quiescence time between outbursts and their X-ray peak intensity.
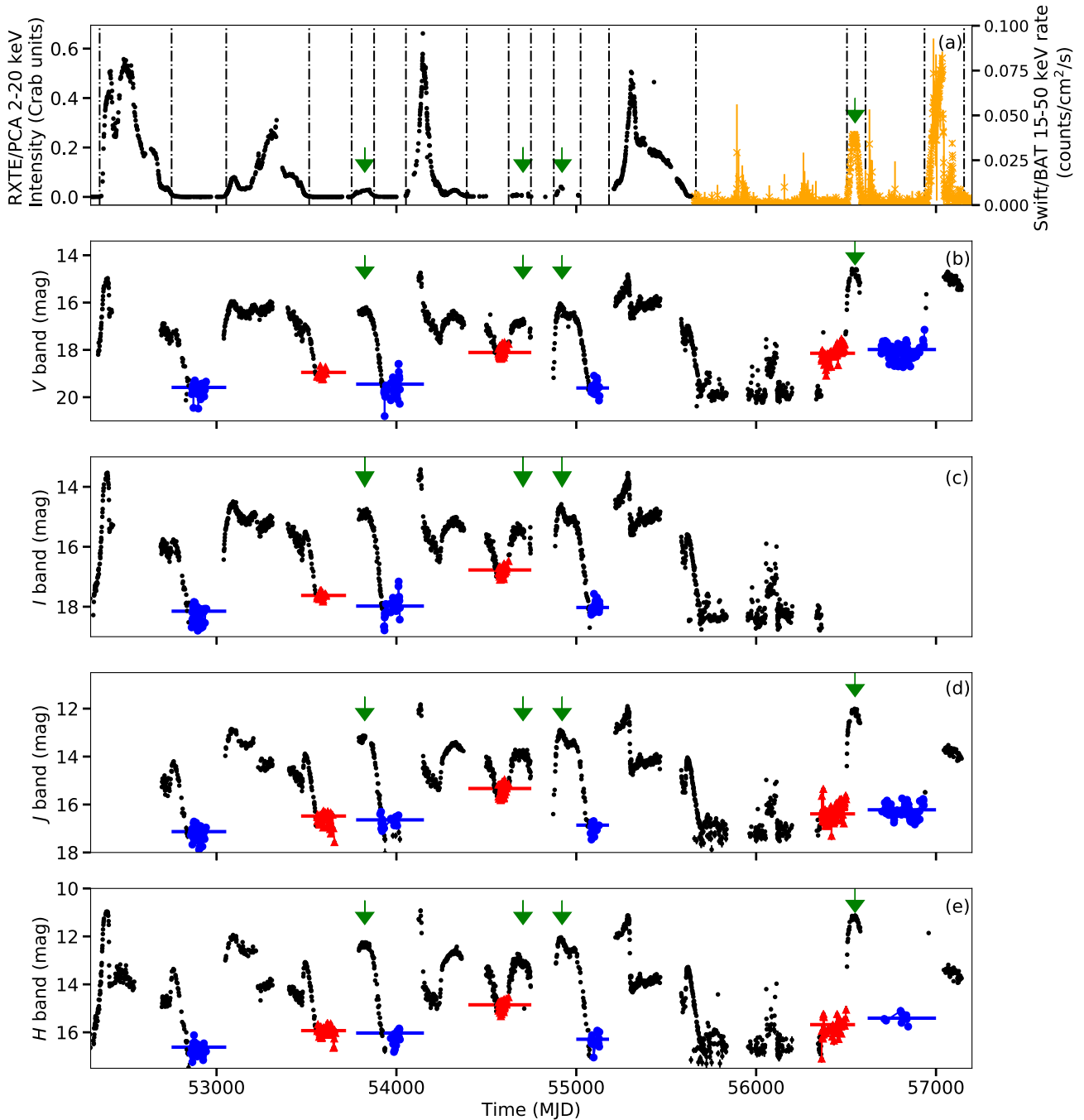
Figure 12. Panel (a): 2002–2010 *RXTE*/PCA light-curve (black symbols) and 2011–2015 *Swift*/BAT light curve (orange symbols). Panel (b): SMARTS *V*-band light curve. Panel (c): SMARTS *I*-band light curve. Panel (d): SMARTS *J*-band light curve. Panel (e): SMARTS *H*-band light curve. Green arrows mark the FT outbursts. Red and blue symbols represent the intervals where the O/IR emission was at the minimum while the source was in quiescence in X-rays before FT and full outbursts, respectively. Blue and red horizontal lines represent the mean values of these intervals. Black dashed lines represent the onset and the offset of the outbursts in X-rays.

This is similar to the result of Campana, Coti Zelati & D'Avanzo (2013) for the NS LMXB Aql X−1. In addition, the fact that some sources have only undergone FT outbursts (see Table A1) suggests that the nature of the outburst, being either an FT or a full outburst, does not depend on the quiescence time between outbursts. Another possible explanation for the lower peak flux in FT outbursts is that the outer disc is not irradiated enough to be involved in the outburst (e.g. different outbursts of Aql X–1, Campana et al. 2013; Güngör,

Güver & Ekşi 2014). Yu, van der Klis & Fender (2004) and Yu & Dolence (2007) also suggested that the total mass of the accretion disc of BH LMXBs influences the peak flux of the LHS of an outburst. They found a positive correlation between the peak flux of the LHS before the hard-to-soft transition and the peak flux of the HSS in full outbursts of XTE J1550−564, Aql X−1, and 4U 1705−44. They speculated that the hard-to-soft transition occurs when the inner disc dominates the emission over the contribution of the outer disc. This
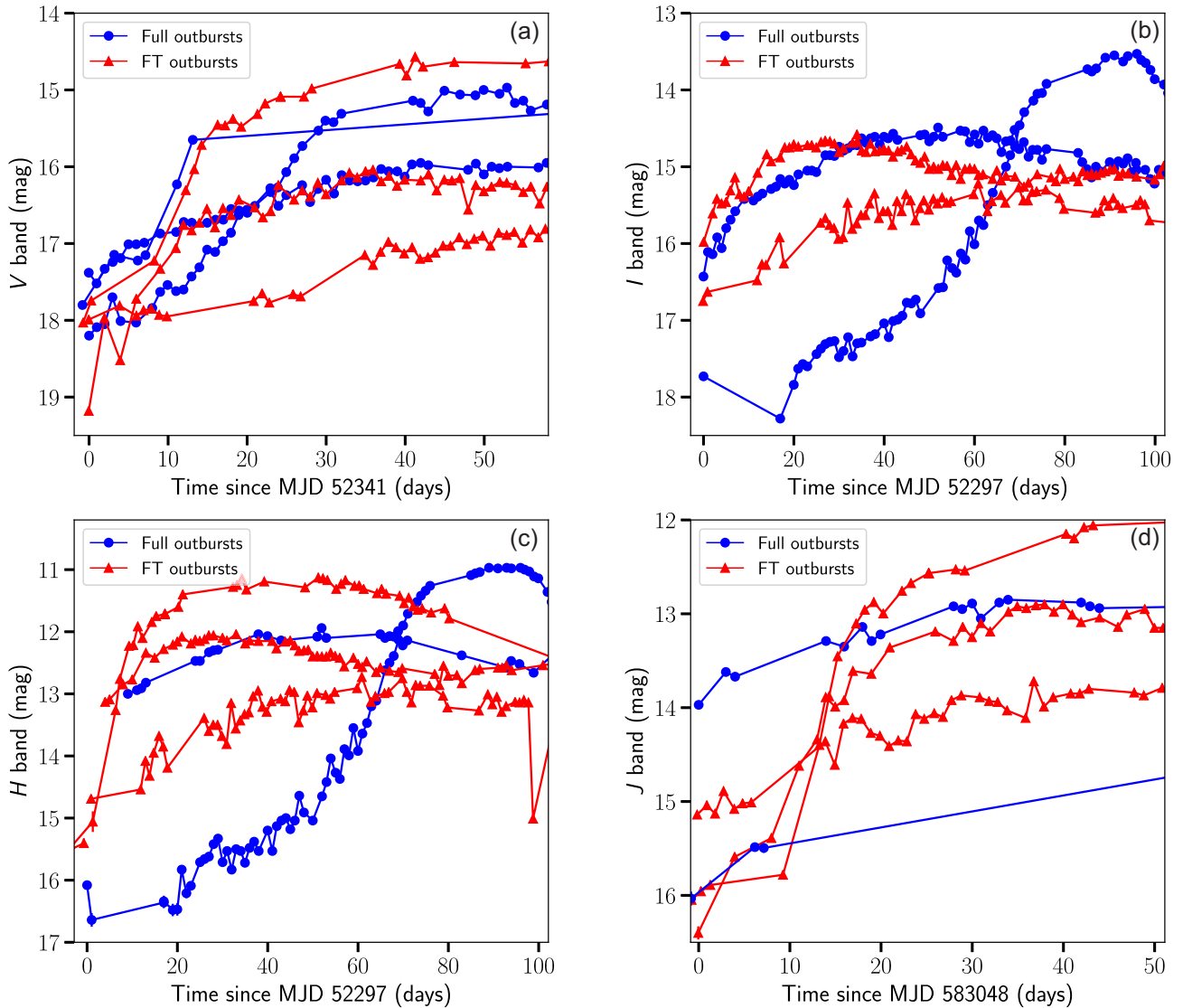
Figure 13. Panel (a): SMARTS *V*-band light curves of the 2002, 2004, 2008, 2009, 2013, and 2014 outbursts of GX 339–4. Panel (b): SMARTS *I*-band light curves of the 2002, 2004, 2008, and 2009 outbursts. Panel (c): SMARTS *J*-band light curves of the 2002, 2004, 2008, 2009, 2013, and 2014 outbursts. Panel (d): SMARTS *V*-band light curves of the 2002, 2004, 2008, 2009, 2013, and 2014 outbursts.

is consistent with the mass of the accretion disc driving the state transitions, since at the beginning of an outburst the mass of the disc is concentrated far from the compact object. Based on these ideas, the main difference between full and FT outbursts would be the mass distribution of the accretion disc, being the outer parts of the accretion disc more massive than the inner parts during an FT outburst. This, however, does not allow us to predict during the first days of an outburst whether it will be an FT or a full outburst.

4.3 FT and full outbursts in O/IR

Comparing the rising part of the O/IR light curves of the outbursts of GX 339−4, we found the same result as in X-rays: we cannot distinguish between full and FT outbursts during the first days. Similarly, we found that both types of outbursts lie in the same regions of the O/IR CMDs. Kosenkov et al. (2020) studied the 2002–2010 outbursts of GX 339−4 and found that both types of outbursts follow the same tracks in O/IR CMDs. In addition, we studied the

CMDs of the outbursts of GX 339−4 in 2013 (FT) and 2014 (full), reaching the same conclusion: both outbursts lie in the same region of the CMD. Similarly to Buxton et al. (2012), we also found that FT outbursts of GX 339−4 in 2006, 2008, and 2009 fall on the top branch of the correlation between O/IR bands, corresponding to the LHS of BH LMXBs. It was also expected, since we know that the FT outbursts of GX 339−4 never left the LHS. The only exception is the FT outburst of 2013. Some observations of this outburst fall on the bottom branch, corresponding to the HSS. One possible explanation for this is that the source started a hard-to-soft transition during this outburst without reaching the HSS. Another possible explanation is that the source started an O/IR transition but not an X-ray transition (Kalemci et al. 2013).

These three results suggest that, as in X-rays, the beginning of both FT and full outbursts are driven by the same physical mechanisms. However, we found that GX 339−4 was brighter before FT outbursts than before full outbursts in O/IR wavelengths. The only exception to this is the full outburst of 2014, in which the O/IR magnitudes are similar to the intervals before FT outbursts.
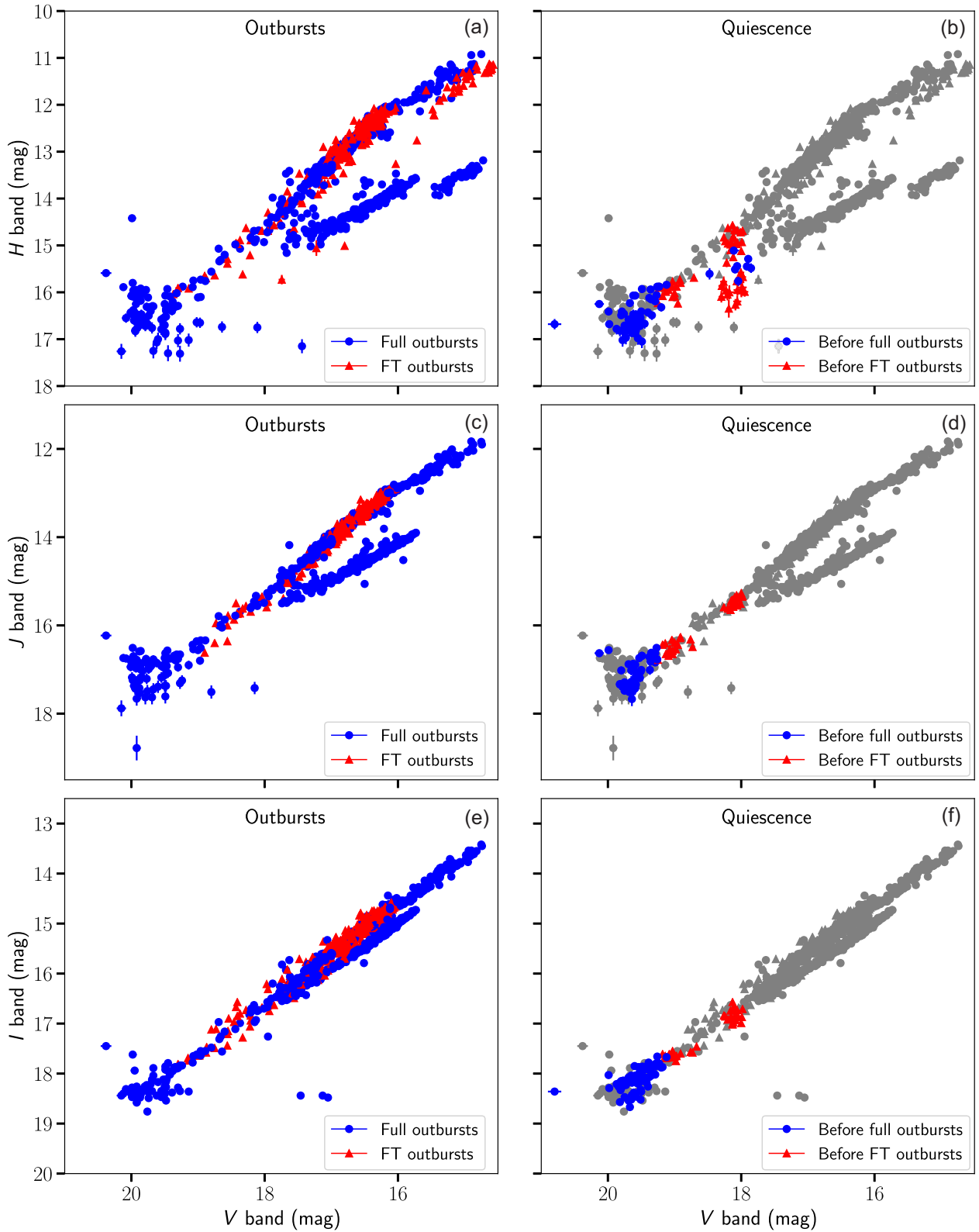
Figure 14. Panels (a) and (b): Correlations between the *V*-band and *H*-band magnitudes corresponding to the outbursts from 2004 to 2014 and the periods of quiescence before outbursts, respectively. Panels (c) and (d): Same as panels (a) and (b) for the *V* and *J* bands. Panels (e) and (f): Same as panels (a) and (b) for the *V* and *I* bands corresponding to the outbursts from 2004 and 2009. Grey points correspond to the data of the outbursts.
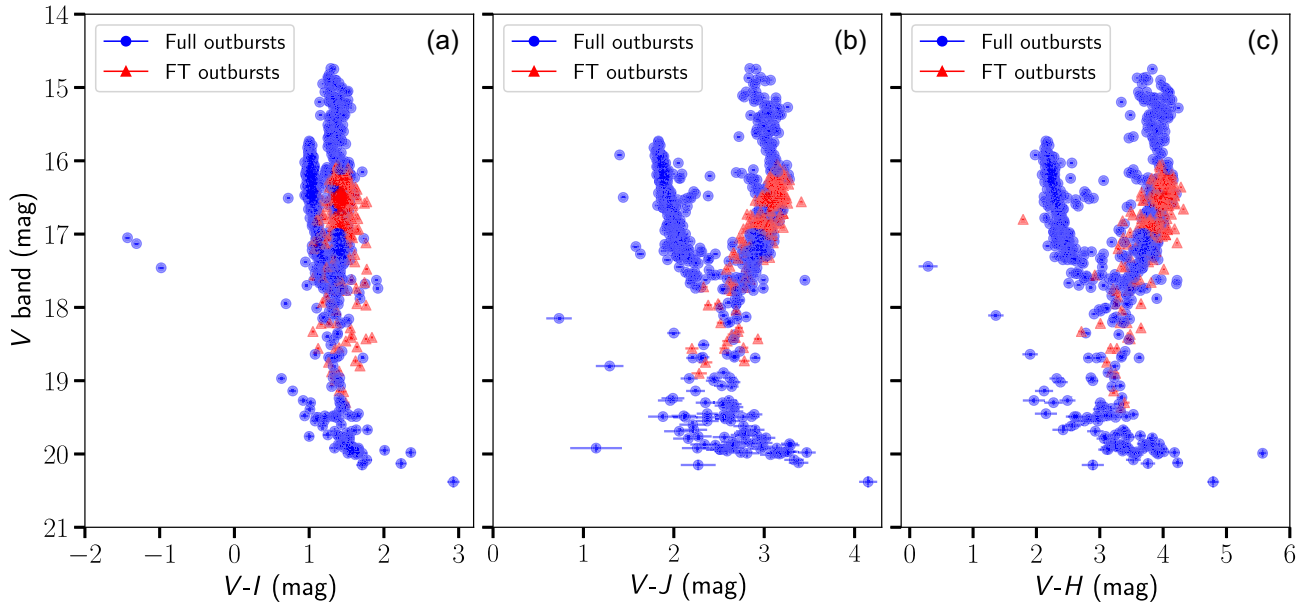
Figure 15. Representative colour–magnitude diagrams of GX 339−4. Blue symbols correspond to the CMDs of full outbursts and red symbols correspond to the CMDs of FT outbursts.

Table 1. Mean magnitude in the *V*, *I*, *J*, and *H* bands of the regions prior to outbursts.

| Type of outburst	Year of the outburst	Mean *V* magnitude (mag)	Mean *I* magnitude (mag)	Mean *J* magnitude (mag)	Mean *H* magnitude (mag)
FT outbursts	2006	18.996 ± 0.005	17.626 ± 0.006	16.57 ± 0.01	15.94 ± 0.01
	2008	18.043 ± 0.003	16.742 ± 0.002	15.399 ± 0.005	14.857 ± 0.005
	2013	18.123 ± 0.004	−	16.146 ± 0.007	15.66 ± 0.02
Full outbursts	2004	19.616 ± 0.006	17.626 ± 0.006	17.15 ± 0.02	16.66 ± 0.02
	2006b	19.273 ± 0.006	17.926 ± 0.005	16.72 ± 0.02	16.14 ± 0.02
	2009b	19.543 ± 0.004	17.998 ± 0.006	16.97 ± 0.03	16.24 ± 0.02
	2014	17.978 ± 0.005	−	16.182 ± 0.009	15.40 ± 0.03
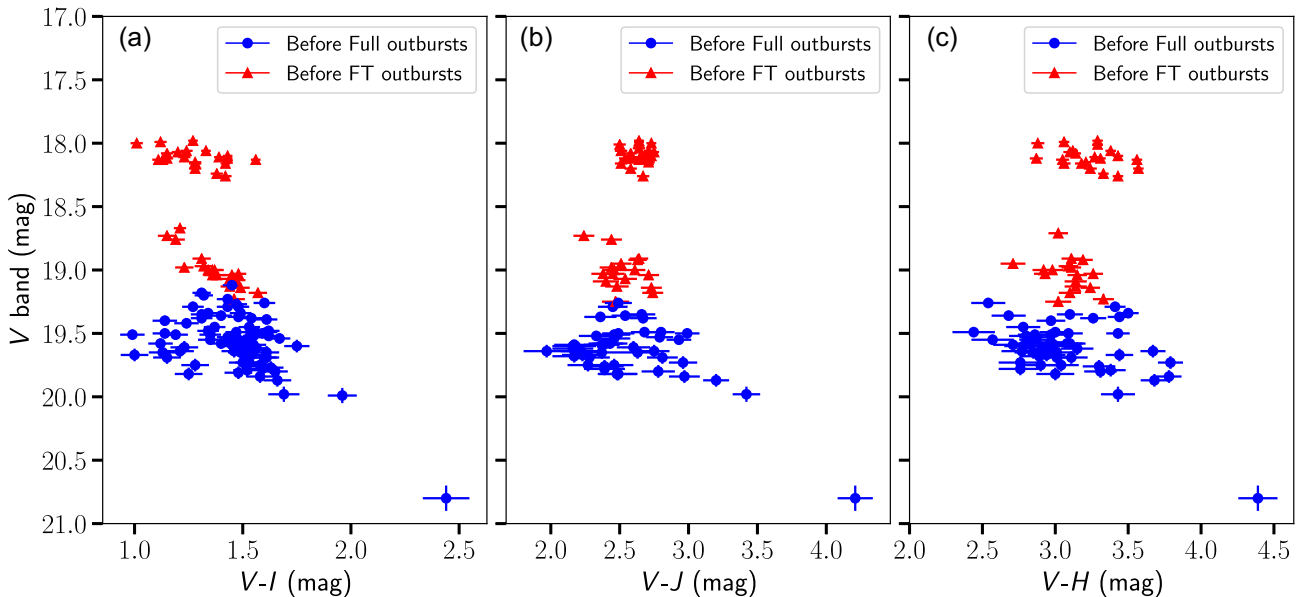
Figure 16. Representative colour–magnitude diagrams of GX 339−4 during quiescence. Blue symbols correspond to the CMDs of quiescence intervals prior to full outbursts and red symbols correspond to the CMDs of quiescence intervals prior to FT outbursts.

The O/IR emission is thought to be produced at the outer parts of the accretion disc irradiated by the X-ray emission from the central object. Subsequent studies suggested that the O/IR emission comes from two components: the accretion disc and a non-thermal component that can be a hot flow, a corona, or a jet, or a combination of all of them (e.g. Fabian et al. 1982; Motch et al. 1983; Kanbach et al. 2001; Gandhi et al. 2008; Casella et al. 2010; Veledina, Poutanen & Vurm 2011). We found that the main difference between FT and full outbursts is that, in quiescence, GX 339−4 is brighter before FT outbursts than before full outbursts. We can consider that the O/IR emission comes from the corona and/or the outer parts of the accretion disc. If we assume that the O/IR emission is mostly originated at the outer parts of the disc, this suggests that the outer part of the disc is more massive before FT outbursts than before full outbursts. This is in agreement with the conclusion achieved from our study of X-ray data, which is that the outer part of the disc is more massive in FT outbursts than in full outbursts. On the other hand, the emission can be mostly originated in the corona, independently of the mass of the accretion disc.

The O/IR emission could also come from the jet. The detection of single frequency radio detections by Gallo et al. (2006, 2014) during quiescence for the systems A0620−00 and XTE J1118+480 suggested the presence of a radio jet in quiescence. Later, Dinçer et al. (2018) found an inverted radio spectrum for A0620−00, reinforcing this idea. Nevertheless, it is difficult to determine the origin of the O/IR emission. Although emission from the accretion disc has been detected in quiescence (e.g. McClintock, Horne & Remillard 1995; Froning et al. 2011), some studies suggest that the emission comes only from the jet (Dinçer et al. 2018). Poutanen, Veledina & Revnivtsev (2014) showed that at low luminosities non-thermal emission from a hot accretion flow could explain the O/IR emission of XTE J1550−564. Similarly, Kosenkov et al. (2020) concluded that the O/IR emission of GX 339−4 could be originated by two non-thermal components: a jet and the hot flow.

In addition to that, Dinçer et al. (2018) found that A0620−00 shows a significant increase in its X-ray flux during quiescence. This has also been observed in other systems, as GS 1354−64 (Koljonen et al. 2016) and Muscae 1991 (Wu et al. 2016). This can be interpreted as the changes in the outer disc and the accretion flow due to the build-up of the disc prior to the onset of a new outburst (Dubus, Hameury & Lasota 2001; Dinçer et al. 2018). This increase is not clearly seen in GX 339−4 in O/IR wavelengths. This could suggest that the accretion rate of GX 339−4 is constant while the source is in quiescence. However, following this idea the mass accretion rate would be higher in quiescence before FT outbursts than before full outbursts. This conclusion is also supported by the estimations of the temperature of the disc in quiescence. Under the assumption that the radius of the disc is constant in quiescence, the mass accretion rate is proportional to T^4. Since the temperature of the disc is higher before the onset of FT outbursts, the mass accretion rate is higher, too.

The evolution of the X-ray power-law index of A0620−00 during quiescence was also studied by Dinçer et al. (2018). The authors found that the photon index does not change with the increasing of the flux. This result suggested that the emission was produced in the same region. However, they suggested that the size of the emission region could be changing. We can link this conclusion with our results. The difference in O/IR magnitude between quiescence prior to FT and full outbursts could be due to a difference in the size of the emitting region. Further studies of O/IR observations while the source is in quiescence before an outburst will show whether this interpretation is correct.

4.4 Inside-out and outside-in outbursts

In the standard disc instability model (DIM), the outbursts are triggered by an instability in the accretion disc (for a review, see Lasota 2001). The instability propagates throughout the disc via two heating fronts: one of them moving inwards and the other moving outwards through the accretion disc (e.g. Smak 1984; Menou, Hameury & Stehle 1999). Depending on the radius at which the outburst is triggered, two types of outburst are distinguished: outside-in and inside-out outbursts. In outside-in outbursts, the ignition occurs close to the outer edge of the accretion disc, and the outward heating front reaches the outer part of the disc faster than the inward heating front reaches the inner parts. This type of outburst produces strongly asymmetric light curves (Smak 1984). In inside-out outbursts, the ignition radius is small and the inward heating front reaches the inner disc radius faster than the outward heating front reaches the outer part of the disc. This type of outburst produces approximately symmetric light curves (Smak 1984). It can happen that the outward heating front fails to propagate to the outer part of the disc because it finds regions of higher densities. Because of that, a cooling front would be developed and it will cool the material, shooting down the outbursts (Hellier 2001). Depending on whether the instability reaches the outer parts of the disc, two subtypes of inside-out outbursts can be distinguished: subtype Ba and subtype Bb (Smak 1984). In subtype Ba outbursts, the instability reaches the outer edge of the disc, while in subtype Bb outbursts the instability does not reach the outer part of the disc. Because of that, the light-curve amplitude and duration of subtype Bb outbursts are shorter. The O/IR light curves of the FT outbursts of GX 339−4 presented in Fig. 12 are more similar to those corresponding to the inside-out outbursts (see fig. 3 in Smak 1984). The light curves corresponding to full outbursts, on the other hand, are more asymmetric, which could mean that the instability that triggers the outburst occurs in the outer part of the accretion disc. If this interpretation is correct, this would mean that both types of outbursts can appear in the same source. If the binary parameters are the same, outside-in outbursts occur at high mass accretion rates, while inside-out outbursts occur at low accretion rates. The fact that the two types are observed in the same source suggests that the mass accretion rate changes from one outburst to another.

4.5 FT outbursts and reflares

Reflares, also known as rebrightenings, rebursts, and mini-outbursts (see e.g. Callanan et al. 1995; Chen, Shrader & Livio 1997; Jonker et al. 2012), are renewed episodes of increased luminosity experienced by some X-ray binaries during the decay of the main outburst, and before returning to quiescence. FT outbursts might sometimes be confused with reflares because both events reach X-ray peak intensities lower than that of main full outbursts. However, they are essentially different. FT outbursts are isolated events similarly to full outbursts.

As discussed in Section 1, FT outbursts never make the transition to the HSS (e.g. Tomsick, Kalemci & Kaaret 2004; Homan et al. 2013, for XTE J1650−500 and MAXI J1659−152, respectively). Instead, during reflares, systems can either stay in the LHS or go through the different spectral states (e.g. Yan & Yu 2017; Cúneo et al. 2020; Zhang et al. 2020). Recent studies of the reflares of MAXI J1348−630 show that they follow a slightly softer track in the HID than the rising part of the main outburst (see fig. 2 of Zhang et al. 2020). While this is a single case, it is a signif-

icant difference with the typical phenomenology observed in FT outbursts.

It has been proposed that reflares and main outbursts are driven by the same physical processes (e.g. Yan & Yu 2017; Cúneo et al. 2020) and that they depend on general accretion physics rather than on the nature of the compact object (e.g. Patruno et al. 2016). The similarities observed in the spectral behaviour of FT and full outbursts, reflares and main outbursts, imply that all these events might be driven by the same mechanisms. However, although it has been widely discussed in the literature (see e.g. Cúneo et al. 2020, and references therein), it is still unknown what powers the renewed activity, either during the decay of an outburst or from quiescence, and which is the mechanism driving and regulating the state transitions.

5 SUMMARY AND CONCLUSIONS

We present the first systematic search for, and study of, the X-ray and O/IR data of FT and full outbursts. We searched in the literature and X-ray archives for data of full and FT outbursts and found that only three sources show enough data to compare the rising part of the outburst: GX 339−4, H 1743−322, and GRS 1739−278. We also looked for O/IR data in the literature and found that the only source with both full and FT outbursts with enough observations during the rise is GX 339−4. We then focused our study on the analysis of the sources with enough observations during the rise of the outbursts: three sources in X-rays (GX 339−4, H 1743−322, and GRS 1739−278) and one source in O/IR wavelengths (GX 339−4). Our results shed light on the behaviour of full and FT outbursts. The summary of our conclusions is the following:

(i) During the first days of the outbursts of the sources studied, X-ray light curves of FT and full outbursts follow similar tracks. In addition, the X-ray HID and PCC diagram tracks are the same. Since the quiescence times before FT and full outbursts are similar, two possible explanations are possible. The first possibility is that the outer part of the accretion disc is more massive than the inner part in an FT outburst, preventing a hard-to-soft state transition. The second option is that the outer part of the disc is not irradiated enough to have a significant effect in the evolution of the outburst.

(ii) We found that the O/IR light curves of FT and full outbursts of GX 339−4 cannot be distinguished during their rising part. However, we found that this system is brighter before the onset of an FT outburst than before the onset of a full outburst. This could be explained by the fact that the mass accretion rate is higher before the onset of FT outbursts. However, the difference between full and FT outbursts could also be the size of the O/IR emission region.

(iii) According to the shape of the O/IR light curves of full and FT outbursts of GX 339−4, the latter would be inside-out outbursts; i.e. the instability is triggered at a radius close to the inner edge of the accretion disc and it cannot reach the outer part of the disc. This could explain the fact that FT outbursts are shorter in time and less bright than full outbursts.

In conclusion, it is not possible to predict whether an outburst will be a full or an FT outburst during the first days of the outbursts only using X-ray data. The key to predict the nature of the outbursts might be the O/IR magnitude of the source while the source is in quiescence, since we have found that GX 339−4 is brighter in O/IR wavelengths before the onset of an FT outburst than before the onset of a full outburst. Although the details of the mechanisms triggering full and FT outbursts remain unknown, it is evident that they are different manifestations of one unique accretion-related process.

Further analysis of the different types of outbursts of X-ray binaries at O/IR wavelengths during quiescence will help to determine whether the type of outburst depends on the accreted mass, the disc geometry, or some other property that still needs to be considered.

DATA AVAILABILITY

The *RXTE* data underlying this article are publicly available in the High Energy Astrophysics Science Archive Research Center (HEASARC) at https://heasarc.gsfc.nasa.gov/db-perl/W3Browse/w3browse.pl. The MAXI data underlying this article are publicly available at http://maxi.riken.jp/top/index.html. The *Swift*/BAT data underlying this article are publicly available at https://swift.gsfc.nasa.gov/results/transients/. The SMARTS data underlying this article until 2011 were published in Buxton et al. (2012) and the data covering from 2011 were provided privately by the SMARTS team.

REFERENCES

Alabarta K. et al., 2020, MNRAS, 497, 3896
Bassi T. et al., 2019, MNRAS, 482, 1587
Belloni T. M., 2010, in Belloni T., ed., Lecture Notes in Physics, Vol. 794, The Jet Paradigm. Springer-Verlag, Berlin, Heidelberg, p. 53
Belloni T. M., Stella L., 2014, Space Sci. Rev., 183, 43
Belloni T. M., Colombo A. P., Homan J., Campana S., van der Klis M., 2002, A&A, 390, 199
Belloni T. M., Homan J., Casella P., van der Klis M., Nespoli E., Lewin W. H. G., Miller J. M., Méndez M., 2005, A&A, 440, 207
Belloni T. M., Motta S. E., Muñoz-Darias T., 2011, Bull. Astron. Soc. India, 39, 409
Brocksopp C., Jonker P. G., Fender R. P., Groot P. J., van der Klis M., Tingay S. J., 2001, MNRAS, 323, 517
Brocksopp C., Bandyopadhyay R. M., Fender R. P., 2004, New Astron., 9, 249
Burke M. J., Gilfanov M., Sunyaev R., 2017, MNRAS, 466, 194
Buxton M. M., Bailyn C. D., Capelo H. L., Chatterjee R., Dinçer T., Kalemci E., Tomsick J. A., 2012, AJ, 143, 130
Callanan P. J. et al., 1995, ApJ, 441, 786

Campana S., Coti Zelati F., D'Avanzo P., 2013, MNRAS, 432, 1695
Capitanio F., Belloni T., Del Santo M., Ubertini P., 2009, MNRAS, 398, 1194
Casella P., Belloni T., Homan J., Stella L., 2004, A&A, 426, 587
Casella P. et al., 2010, MNRAS, 404, L21
Chen W., Shrader C. R., Livio M., 1997, ApJ, 491, 312
Corbel S., Coriat M., Brocksopp C., Tzioumis A. K., Fender R. P., Tomsick J. A., Buxton M. M., Bailyn C. D., 2013, MNRAS, 428, 2500
Cúneo V. A. et al., 2020, MNRAS, 496, 1001
Curran P. A., Chaty S., 2013, A&A, 557, A45
de Haas S. E. M. et al., 2020 MNRAS, 502, 521
DePoy D. L. et al., 2003, in Iye M., Moorwood A. F. M., eds, Proc. SPIE Conf. Ser. Vol. 4841, Instrument Design and Performance for Optical/Infrared Ground-Based Telescopes. SPIE, Bellingham, p. 827
Dinçer T., Bailyn C. D., Miller-Jones J. C. A., Buxton M., MacDonald R. K. D., 2018, ApJ, 852, 4
Done C., Gierliński M., Kubota A., 2007, A&AR, 15, 1
Dubus G., Hameury J. M., Lasota J. P., 2001, A&A, 373, 251
Dunn R. J. H., Fender R. P., Körding E. G., Belloni T., Cabanac C., 2010, MNRAS, 403, 61
Esin A. A., McClintock J. E., Narayan R., 1997, ApJ, 489, 865
Fabian A. C., Guilbert P. W., Motch C., Ricketts M., Ilovaisky S. A., Chevalier C., 1982, A&A, 111, L9
Fender R. P., Homan J., Belloni T. M., 2009, MNRAS, 396, 1370
Ferrigno C., Bozzo E., Del Santo M., Capitanio F., 2012, A&A, 537, L7
Froning C. S. et al., 2011, ApJ, 743, 26
Fürst F. et al., 2015, ApJ, 808, 122
Gallo E., Fender R. P., Miller-Jones J. C. A., Merloni A., Jonker P. G., Heinz S., Maccarone T. J., van der Klis M., 2006, MNRAS, 370, 1351
Gallo E. et al., 2014, MNRAS, 445, 290
Gandhi P. et al., 2008, MNRAS, 390, L29
Güngör C., Güver T., Ekşi K. Y., 2014, MNRAS, 439, 2717
Heil L. M., Uttley P., Klein-Wolt M., 2015, MNRAS, 448, 3339
Hellier C., 2001, Cataclysmic Variable Stars. Springer-Verlag, London
Homan J., Belloni T., 2005, Ap&SS, 300, 107
Homan J., Wijnands R., van der Klis M., Belloni T., van Paradijs J., Klein-Wolt M., Fender R., Méndez M., 2001, ApJS, 132, 377
Homan J., Fridriksson J. K., Jonker P. G., Russell D. M., Gallo E., Kuulkers E., Rea N., Altamirano D., 2013, ApJ, 775, 9
Hynes R. I., Mauche C. W., Haswell C. A., Shrader C. R., Cui W., Chaty S., 2000, ApJ, 539, L37
in't Zand J. J. M. et al., 2002, A&A, 390, 597
Jahoda K., Markwardt C. B., Radeva Y., Rots A. H., Stark M. J., Swank J. H., Strohmayer T. E., Zhang W., 2006, ApJS, 163, 401
Jonker P. G., Miller-Jones J. C. A., Homan J., Tomsick J., Fender R. P., Kaaret P., Markoff S., Gallo E., 2012, MNRAS, 423, 3308
Kalemci E., Dinçer T., Tomsick J. A., Buxton M. M., Bailyn C. D., Chun Y. Y., 2013, ApJ, 779, 95
Kanbach G., Straubmeier C., Spruit H. C., Belloni T., 2001, Nature, 414, 180
Koljonen K. I. I., Russell D. M., Corral-Santana J. M., Armas Padilla M., Muñoz-Darias T., Lewis F., Coriat M., Bauer F. E., 2016, MNRAS, 460, 942
Kosenkov I. A., Veledina A., Suleimanov V. F., Poutanen J., 2020, A&A, 638, A127
Kuulkers E., van der Klis M., Oosterbroek T., Asai K., Dotani T., van Paradijs J., Lewin W. H. G., 1994, A&A, 289, 795
Lasota J.-P., 2001, New Astron. Rev., 45, 449
Lewis F., Russell D. M., Shahbaz T., 2012, Astron. Telegram, 4162, 1
Maccarone T. J., Russell D. M., Glamorgan F. L., 2012, Astron. Telegram, 4247, 1
McClintock J. E., Horne K., Remillard R. A., 1995, ApJ, 442, 358
McConnell M. L. et al., 2002, ApJ, 572, 984
Méndez M., van der Klis M., 1997, ApJ, 479, 926
Menou K., Hameury J.-M., Stehle R., 1999, MNRAS, 305, 79
Mitsuda K. et al., 1984, PASJ, 36, 741
Motch C., Ricketts M. J., Page C. G., Ilovaisky S. A., Chevalier C., 1983, A&A, 119, 171

Motta S. E., 2016, Astron. Nachr., 337, 398
Motta S. E., Muñoz-Darias T., Casella P., Belloni T., Homan J., 2011, MNRAS, 418, 2292
Motta S. E., Homan J., Muñoz Darias T., Casella P., Belloni T. M., Hiemstra B., Méndez M., 2012, MNRAS, 427, 595
Muñoz-Darias T., Motta S., Belloni T. M., 2011, MNRAS, 410, 679
Patruno A., Maitra D., Curran P. A., D'Angelo C., Fridriksson J. K., Russell D. M., Middleton M., Wijnand s R., 2016, ApJ, 817, 100
Plant D. S., Fender R. P., Ponti G., Muñoz-Darias T., Coriat M., 2014, MNRAS, 442, 1767
Poutanen J., Veledina A., Revnivtsev M. G., 2014, MNRAS, 445, 3987
Remillard R. A., McClintock J. E., 2006, ARA&A, 44, 49
Remillard R., Levine A. M., Morgan E. H., Markwardt C. B., Swank J. H., 2006, Astron. Telegram, 714
Rodriguez J., Corbel S., Kalemci E., Tomsick J. A., Tagger M., 2004, ApJ, 612, 1018
Shakura N. I., Sunyaev R. A., 1973, in Bradt H., Giacconi R., eds, Proc. IAU Symp. 55, X- and Gamma-Ray Astronomy. D. Reidel, Dordrecht, p. 155
Smak J., 1984, Acta Astron., 34, 161
Sriram K., Rao A. R., Choi C. S., 2013, ApJ, 775, 28
Subasavage J. P., Bailyn C. D., Smith R. C., Henry T. J., Walter F. M., Buxton M. M., 2010, in Silva D. R., Peck A. B., Soifer B. T., eds, Proc. SPIE Conf. Ser. Vol. 7737, Observatory Operations: Strategies, Processes, and Systems III. SPIE, Bellingham, p. 77371C
Sunyaev R. A., Titarchuk L. G., 1980, A&A, 86, 121
Sunyaev R. A., Truemper J., 1979, Nature, 279, 506
Tetarenko B. E., Sivakoff G. R., Heinke C. O., Gladstone J. C., 2016, ApJS, 222, 15
Titarchuk L., 1994, ApJ, 434, 570
Tomsick J. A., Kalemci E., Kaaret P., 2004, ApJ, 601, 439
Uttley P., Klein-Wolt M., 2015, MNRAS, 451, 475
van der Klis M., 1989, ARA&A, 27, 517
van der Klis M., 2000, ARA&A, 38, 717
Veledina A., Poutanen J., Vurm I., 2011, ApJ, 737, L17
Wijnands R., Homan J., van der Klis M., 1999, ApJ, 526, L33
Williams D. R. A. et al., 2020, MNRAS, 491, L29
Wu J., Orosz J. A., McClintock J. E., Hasan I., Bailyn C. D., Gou L., Chen Z., 2016, ApJ, 825, 46
Yan Z., Yu W., 2017, MNRAS, 470, 4298
Yu W., Dolence J., 2007, ApJ, 667, 1043
Yu W., van der Klis M., Fender R., 2004, ApJ, 611, L121
Zdziarski A. A., Poutanen J., Paciesas W. S., Wen L., 2002, ApJ, 578, 357
Zdziarski A. A., Gierliński M., Mikołajewska J., Wardziński G., Smith D. M., Harmon B. A., Kitamoto S., 2004, MNRAS, 351, 791
Zhang W., Giles A. B., Jahoda K., Soong Y., Swank J. H., Morgan E. H., 1993, in Siegmund O. H., ed., Proc. SPIE Conf. Ser. Vol. 2006, EUV, X-Ray, and Gamma-Ray Instrumentation for Astronomy IV. SPIE, Bellingham, p. 324
Zhang L. et al., 2020, MNRAS, 499, 851

SUPPORTING INFORMATION

Supplementary data are available at *MNRAS* online.

APPENDIX A. TABLE WITH ALL THE OUTBURSTS OF THE DIFFERENT SOURCES INCLUDED IN THIS PAPER
APPENDIX B. O/IR INTERVALS SELECTED TO STUDY FT AND FULL OUTBURSTS DURING QUIESCENCE

Please note: Oxford University Press is not responsible for the content or functionality of any supporting materials supplied by the authors. Any queries (other than missing material) should be directed to the corresponding author for the article.

This paper has been typeset from a TEX/LATEX file prepared by the author.